International Journal of Environmental Research (2021) 15:543–558
https://doi.org/10.1007/s41742-021-00333-1

RESEARCH PAPER

Development of Functionalized Activated Carbon for Uranium Removal from Groundwater

Mahmoud O. Abd El-Magied[1] · Ali M. Hassan[2] · Ibrahim K. El-Aassy[1] · Hamdi M. H. Gad[3] · Mohamed A. M. Youssef[1] · Tarek F. Mohammaden[1]

Received: 19 January 2021 / Revised: 19 March 2021 / Accepted: 29 March 2021 / Published online: 10 April 2021

Abstract

Some water wells used for drinking and other human activities in southwest Sinai, Egypt, recorded higher concentrations of uranium than the permissible levels. This paper focuses on uranium removal from groundwater. This target was utilized to develop an efficient and cost-effective graphite adsorbent (Graphite/AC), which was further altered by oxidation (O/AC) and amination (N/O/AC). Studying the controlling factors that affect the removal of uranium by O/AC and N/O/AC samples including, contact time, adsorbent amount, initial uranium concentration, solution pH, operational temperature, and the interfering of metal ions were tested and discussed. Dynamic and thermodynamics studies were achieved to predicate the performance of N/O/AC and O/AC for U(VI) removal from the groundwater samples. The activity of radionuclide (^{238}U-series, ^{232}Th-series and ^{40} K) and radioactive hazards indices of the groundwater samples were calculated and discussed. The developed materials showed good potential for the treatment of aqueous systems polluted by uranium, with 100 mg/g as maximum capacity. The thermodynamic parameters refer to the spontaneity and endothermic nature of the U(VI) ions adsorption process. A solution of 0.25 M HNO_3 was found to be good enough for desorbing the adsorbed U(VI) from the adsorbents (96.8%). The positive effect of the used adsorbents (on the removal or minimizing the radioactive daughters consequently reduction of the hazard indices values) should be noted; this effect will be very helpful and effective with the old-age uranium concentrations.

Introduction

Uranium (U) is released into the environment by various activities such as weathering activity of the parent igneous rocks, agricultural runoff from farmland, and wastewater. Uranium, as an inorganic pollutant, is a toxic, radioactive, non-biodegradable and is known for its serious human health impacts. Generally, the toxicity of uranium depends on exposure type (acute or chronic), absorbed dose, and the chemical form of the uranium (Friedlander et al. 1981; Cheremisinoff 2002; Loveland et al. 2006). The handling of uranium results in hazards either by ingestion of alpha particle emitted which can be fatal when kidney, bone, and liver are permanently compromised on a wide scale, or proximity to gamma-ray emitters during working hours. Uranium can impair numerous body physiology, systems, and organs in the body such as kidneys, liver, colon, nervous, urinary, enzymatic, gastrointestinal, and energy production; hence, it can cause serious health problems for humans (Friedlander et al. 1981; Cheremisinoff 2002; Loveland et al. 2006).

The recovery of uranium is crucial to minimize its environmental release. So, their extraction and separation from water sources becomes a very significant task. The removal of uranium, as a contaminant in water, is exceptionally complicated due to several factors that must be considered, such as pH, temperature, solution composition, and salinity. Many uranium removal systems have been considered to conform to the required waste effluent disposal regulations. The most popular systems are chemical precipitation, chemical oxidation treatment, biological treatment, Solvent extraction, and adsorption (Wu et al. 2018; Mokhine et al. 2020; Bai et al. 2020; Singhal et al. 2020; Tang et al. 2020; Amini

✉ Mahmoud O. Abd El-Magied
mahmoud_nma@yahoo.com

[1] Nuclear Materials Authority, El Maadi, P.O. Box 530, Cairo, Egypt

[2] Chemistry Department, Faculty of Science, Al-Azhar University, Cairo, Egypt

[3] Egyptian Atomic Energy Authority, Cairo, Egypt

Graphic Abstract

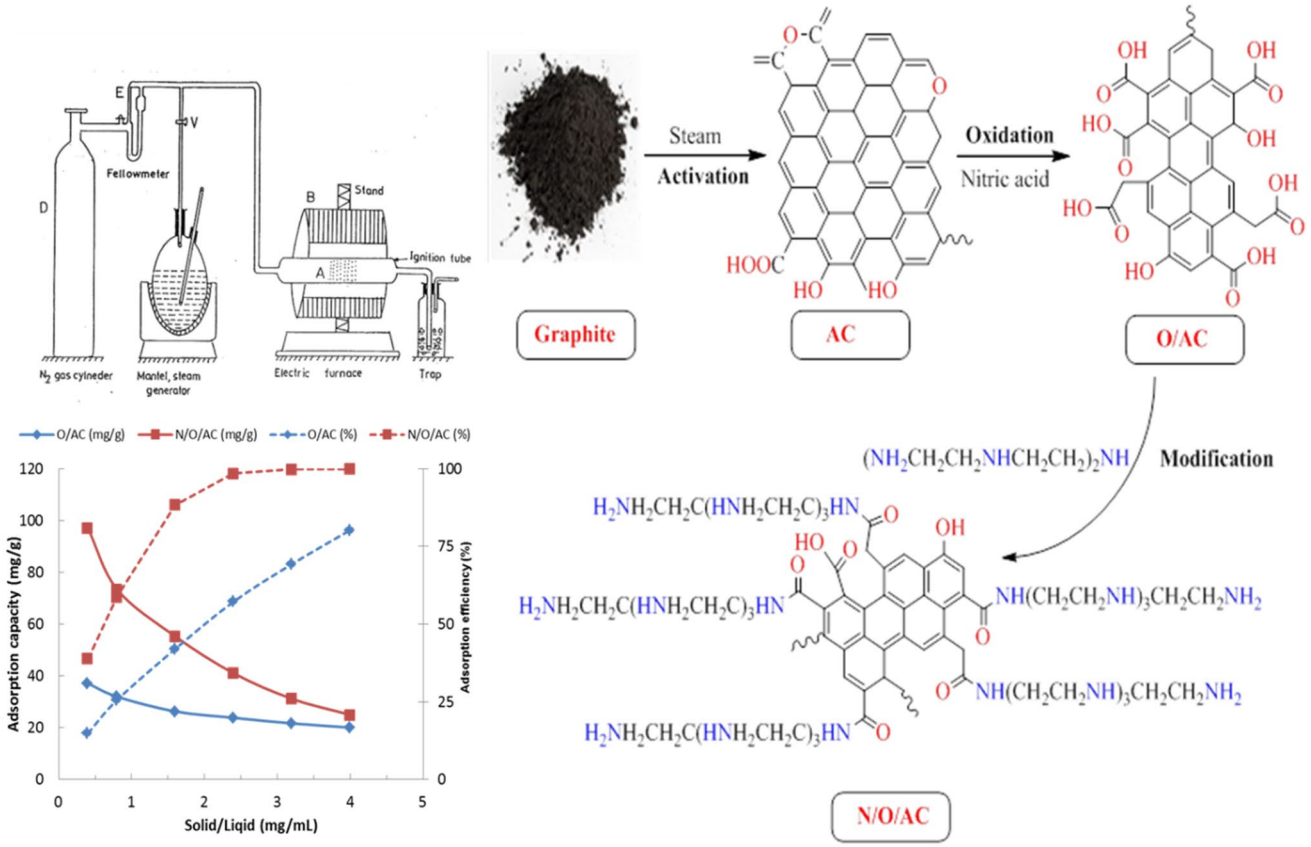

Keywords Activated carbon · Removal · Radioactive · Kinetic · Graphite

et al. 2021). Chemical precipitation is a known remediation technique that involves the precipitation of uranium with a carrier element. The chemical oxidation treatment contains selectively modify the pollutant's toxicity by way of altering its chemical nature. The process requires the utilization of strong chemical oxidizers to destroy and remove organic pollutants within polluted wastewaters. The biological treatment contains degradation or transformation of organic/inorganic compounds in wastewater by biological means, i.e., using specific microorganisms such as aerobic and anaerobic bacteria and fungi to biodegrade waste. Solvent extraction is based on uranium distribution between two or more essentially immiscible solvents. Several extractants have been developed with various ligands like crown ethers, phosphonic acid-based ligands, amine, β-ketones, and calixarenes (Wu et al. 2018; Mokhine et al. 2020; Bai et al. 2020). Solvent extraction offers several advantages which include its simplicity and fast kinetics. On the opposite side, solvent extraction has some drawbacks, including the requirement of the costly amount of organic solvents and the generation of toxic organic waste.

Adsorption is an essential technique in heavy metal extraction and cleaning (Donia et al. 2011a and b; Tag El-Din et al. 2018a and b; El-Said et al. 2018). The fundamental rule of adsorption is the exchange or transfer of ions or molecules from the solution to the adsorbent active sites. Several adsorbents were used to separate uranium from wastewater, such as styrene/divinylbenzene, aluminosilicate, graphene oxide, nanoparticles, glycidyl methacrylate, carbon quantum dots, and activated carbon (Elshehy 2017; Mahmoud et al. 2020; Singhal et al. 2020; Tang et al. 2020; Amini et al. 2021). Recently, natural adsorbents such as activated carbon (AC), clays, chitosan, and silica have attained more attention. Among the natural adsorbents, activated carbon-based sorbents have great attention.

AC has a simple and cheap synthesis route, long usable lifetimes, elevated internal surface area and porosity, chemical, and thermal stability. AC has been prepared

from different sources including rice straw, olive stones, charcoal, lotus stalks, pecan nutshell, polystyrene waste, biomass, and lignin (Cheremisinoff 2002; Alahabadi et al. 2020; Saha et al. 2020). The selection of a raw material for Ac production depends on its inorganic content, application of the manufactured AC, and kind of the adsorbate. Due to their simple and cheap routes of synthesis, the activated carbon represents a reasonable alternative for developing efficient and cost-effective adsorbents for uranium removal from wastewaters.

Groundwater is the main source of usable water, in the drinking and agriculture process, in many areas in Egypt, especially in the desert areas. Some of the groundwater wells in the Wadi Naseib area, southwestern Sinai, Egypt are used for drinking and other human activities. Occasionally, this groundwater records a high concentration of uranium and other metals ion. These metals come to the groundwater due to the aqueous/rock interactions and rain effect that leaches some metals from surrounding rocks then penetrates the underground as a feeding source for the water wells.

The current work aimed to reduce uranium in the water wells to its safe limits of concentration, which is a vital human health issue. To conduct this goal, highly cost-effective activated carbons, as adsorbents, were prepared from graphite. The adsorbents were fully characterized and applied for uranium removal for aqueous media. To conduct the optimum controlling factors that affect the adsorption process, several synthetic solutions of the target hazards contaminants were prepared and tested with the prepared activated carbon samples. The factors examined were solution pH, solid–liquid, time, U(VI) concentration, amount of AC, and operational temperature. Besides, several isotherm models were applied to test the equilibrium relationship between the solid- and liquid-phase concentration of the contaminants. Also, different kinetic models were used to identify the dynamics process. In an application step, the achievable optimum conditions were applied to the groundwater samples.

Materials and Methods

Arsenazo III, N'-[2-[2-(2-Aminoethylamino)ethylamino] ethyl]ethane-1,2-diamine (Tepa, ≥ 95.0%), HCl (37%), HNO_3 (68–70%), NaOH (≥ 98%), and ethanol (≥ 99%) were Sigma-Aldrich products. Uranyl Acetate, $UO_2(OCOCH_3)_2{\cdot}2H_2O$, was obtained from Electron Microscopy Science and was used as sources for U(VI). All other chemicals were Prolabo products and were used as received. Adjustments were performed using 0.1 N HCl and 0.1 N NaOH solutions; U(VI) concentration was estimated spectrophotometrically using the Arsenazo III method (Marczenko 1979).

Development of Functionalized Activated Carbon

Graphite/AC was re-synthesized, from graphite, according to our previous work, supplementary information (SI) (Abd El-Magied et al. 2017). A known weight of the obtained Graphite/AC samples was soaked in (1:1) HCl solutions for 24 h at room temperature to remove the adsorbed impurities. the Graphite/AC was decanted and washed with de-ionized water.

The purified Graphite/AC was oxidized with 100 mL of HNO_3 solution (5 M) at 75 °C, for 6 h. The product was filtered out, washed and dried at 105 °C. The resulting oxidized Graphite/AC is called O/AC.

A 20 g of the O/AC was reacted with 80 mL of N'-[2-[2-(2-Aminoethylamino)ethylamino]ethyl]ethane-1,2-diamine, Tepa, dissolved in toluene (80 mL) at 80 °C for 8 h. The obtained amino form (N/O/AC) was filtered, washed, and then dried. The features of O/AC and N/O/AC were evaluated by numerous approaches. O/AC and N/O/AC surface features were examined using SEM (model XL 30 ESEM). A Perkin-Elmer FTIR-1600 series infrared spectrometer recorded the infrared spectra of prepared activated carbon.

Brunauer, Emmet, and Teller (BET) surface areas were obtained from N_2 adsorption isotherm data collected at 77 K (Quantachrome NOVA 2200C, USA). Before analysis, 0.5 g of the O/AC and N/O/AC samples was dried overnight at 393 K and subsequently outgassed at 573 K for 20 h.

One gram of the dried O/AC or N/O/AC samples was placed in a porcelain crucible, which was placed at 800 °C on a rotating disc (for 30 min.), ensuring full ignition of all carbonate matter. During one hour, the crucible was moved into the muffle more deeply and the temperature was kept between 750 and 800 °C for 1 h, then the crucible was moved cool to in a desiccator. The ash content is indicated as a percentage of the adsorbent in origin as follows:

$$\text{Ash} = \frac{\text{Weight of ash}}{\text{Weight of adsorbent}} \times 100 \quad (1)$$

The content of C, H, N, S, O (%) was analyzed by the elemental analyzer (ELEMENTAR VARIO EL III). Adsorbents pH was measured by adding 1 g of adsorbent powder to 50 ml of bi-distilled water (pH 7.0), and heated to 90 ^{0}C; it was then cooled down to 20 ^{0}C where its pH was determined electrometrically. The pH value was accurately measured within the error of ± 0.01 using a digital pH-meter of the Digimed DM-21 type (Japan).

Adsorption Studies

The pH impact on the sorption of uranium by the activated carbon was evaluated in the range 1–7. Uptake experiments were done by placing 0.02 g of the activated carbon in a round flask containing 20mL of the U(VI) solution (50 mg/L). The contents of the flask were shaken on a Vibromatic-384 shaker for 24 h. . After filtration, the filtrates were analyzed to determine the adsorption capacity. The adsorbents uptake is expressed by the sorption capacity (q_e) using Eq. 2 (Yousef et al. 2020).

$$q = \frac{(C_0 - C_e) \times (V)}{\text{mass of adsorbent (g)}}, \quad (2)$$

where q_e is the sorption capacity (mg/g), C_o is the U(VI) initial concentration (mg/L), C_e is U(VI) concentration in the liquid phase at equilibrium time (mg/L) and V is the volume (L).

The effect of initial uranium concentrations (50–300 mg/g) was studied at 298–313 K. Suspensions containing activated carbon (0.02 g) in 20 ml of 50 mg/L U(VI) solutions were shaken for diverse time interims (5–240 min).

Different adsorbent weights (0.01 – 0.2g) were put in a series of bottles. To each bottle, a 25 ml of U(VI) solution (100 mg L^{-1}) was added. The bottles were shaken for 3 h at room temperature, then they were filtrated and the U(VI) residual levels were decided within the filtrate.

Desorption Investigation

Desorption tests were conducted on the active carbon samples which were loaded by the pollutants. The desorption was examined by adding 25 ml of bi-distilled water and 0.1 M of the nitric acid, hydrochloric acid, sodium hydroxide, and sulfuric acid solution; then the mixtures were shacked for a predetermined time interval. Determination of the desorbed amounts of the uranium was similarly carried out as in the sorption investigations.

Application of the Activated Carbon for Groundwater Sample

Water samples (Well-1, Well-2, Well-Zeid, and Well-Oda) were collected and transferred to polyethylene bottles and 5 ml of HNO_3 to each liter of water. The chemistry of the collected water samples was identified using different analytical techniques. Before and after contact with active carbon, the collected samples were analyzed with the uranium content by inductively coupling plasma optical emission spectroscopy (ICP-OES prism, Teledyne technologies).

Results and Discussions

Preparation of the Adsorbents

The development of AC using one-step activation, which means that the carbonaceous raw material from the beginning is exposed to the steam (activation agent), and carbonization and activation occur simultaneously. Figure 1 shows a sketch of the tube furnace utilized within the development of Graphite/AC from graphite.

The tube furnace contains a reactor (A) stainless steel tube (4 cm inner diameter) fitted with screw caps of narrow tubes and an internal net near one end. This tube was introduced into a calibrated tubular electric furnace (B). Second, O/AC was prepared from Graphite/AC by chemical modification through Nitric acid treatment. The concentration and nature of the O/AC surface functional group can be modified by tailoring it through suitable chemical or thermal post-treatment methods. This type of treatment is generally used to oxidize the porous carbon surface to enhance its acidic property, improve the material surface hydrophilic and eliminate elemental minerals of it. Finally, O/AC was modified with N'-[2-[2-(2-Aminoethylamino)ethylamino] ethyl]ethane-1,2-diamine to produce N/O/AC adsorbent. The synthesis route of active carbon and its further modification is presented in Fig. 1.

Characterization of the Adsorbents

Table 1 lists some physical and chemical features of O/AC and N/O/AC (surface area analysis; elemental analysis; amine and carboxyl content (mmol/g)). The carbon yield of O/AC was found to be 85%, respectively, which was calculated as the final weight of the produced activated carbon (after activation, washing, and drying)/ raw material's initial weight.

The FT-IR spectra of O/AC showed the characteristic bands of OH (3424 cm^{-1}), CH_2 (2377 cm^{-1}), CO (1625 cm^{-1}), and CH (755 cm^{-1}) groups. The spectrums of N/O/AC shows the OH's signature peaks (3434 cm^{-1}), CH_2 (2364 cm^{-1}), NH_2 (2037 cm^{-1}), NH (1429 cm^{-1}), and CN (1087 cm^{-1}) groups, which confirms the successful grafting of the amino-groups onto the O/AC, Fig. 2 (Coates 2000).

The SEM images show the surface of O/AC and N/O/AC before and after uranium adsorption. Adsorption of uranium on the surfaces of the N/O/AC was confirmed through the variations in surface features after loading by uranium as seen in the SEM images, Fig. 3. Further verification was attained by the analysis EDX of the loaded adsorbents. The EDX charts of adsorbents after contact with the uranium

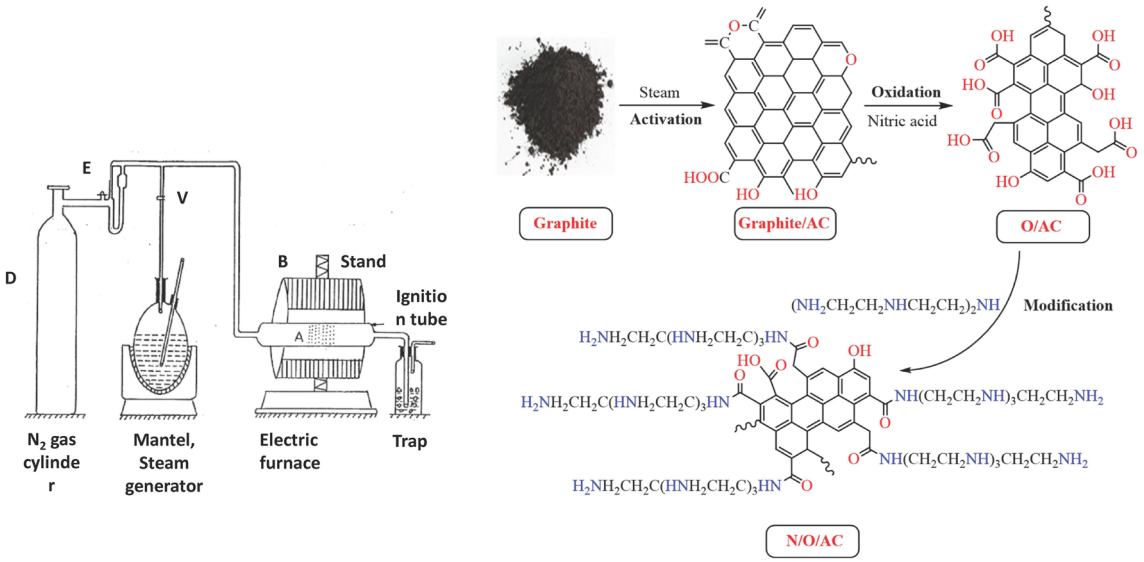

Fig.1 A schematic diagram showing the synthesis of graphite-activated carbons and the used system in the steam activation

ions proved that it retained a high amount of uranium ions (SI, Figs. S1 and S2).

Effect of pH

Uranium ions adsorption was tested under variable pH values (1–6) (Fig. 4) to verify the pH role. U(VI) adsorption showed a gradual increase with the pH increasing. At low pH, the amino-activated carbon is in a fully protonated form. Thus, the uranium removal performance of the amine-activated carbon is insignificant at lower pH values. Also, the carboxylic acids are protonated at lower pH values and are less effective donors. While the pH increases, the protonation of nitrogen and oxygen donor's atoms decreases; adsorption increased accordingly. The maximum adsorption values of 32.45 and 73.41 mg/g were recorded at pH 4.5 and 5 for O/AC and N/O/AC, respectively. In aqueous solution, various oligomeric and monomeric hydrolyzed species of U(VI) were reported. These include $[UO_2OH]^+$, $[(UO_2)_3(OH)_4]^{2+}$, $[(UO_2)_3(OH)_5]^+$, $[(UO_2)_2(OH)_2]^{2+}$, $[(UO_2)_2OH]^{3+}$, $[(UO_2)_3(OH)]^{5+}$, $[(UO_2)_4(OH)]^{7+}$, $[UO_2(OH)_4]^{2-}$ and $[(UO_2)_3(OH)_7]^-$. The suggested mode of interaction between uranium ions (positively charged species) and the activated carbon (Scheme 2) is as follows:

$$2N/O/AC.COOH + UO_2^{2+} + 2H_2O \rightarrow (N/O/AC.COO)_2UO_2 + 2H_3O^+, \quad (3)$$

$$N/O/AC.COOH + UO_2^{2+} \rightarrow [N/O/AC.COOHUO_2]^{2+}, \quad (4)$$

$$N/O/AC.NH_2 + UO_2^{2+} \rightarrow [N/O/AC.NH_2UO_2]^{2+}. \quad (5)$$

The observed low adsorption of U(VI) would be strongly expected at low pH values (1-3) due to the protonation of the adsorbent active sites (OH, NH_2, and COOH).

Effect of time and Adsorption Kinetics

The sorption capacities of the N/O/AC and O/AC and at different contact times were examined. Batch kinetics

Table 1 Characterization of adsorbents physically and chemically

Parameters	O/AC	N/O/AC
Carbon yield (%)	85	85
Ash content (%)	2.70	1.69
BET surface area (m^2/g)	30.282	8.187
Langmuir surface area (m^2/g)	48.029	15.285
Micropore surface area (m^2/g)	36.512	8.786
Pore volume (total) (cm^3/g)	0.0102	0.0022
Micropore volume (cm^3/g)	0.0067	0.0001
Mesopores volume (cm^3/g)	0.0035	0.0011
Average pore radius (Å)	90.1	60.2
Average Particle Size (Å)	1096.51	3483.96
C %	70.52	63.16
H %	0.45	0.73
N %	< 0.01	3.28
O % (by difference)	29.52	26.15
Amin content (mmol/g)	< 0.01	1.2
Carboxyl group (mmol/g)	2.4	1.5

experiments were performed for different interval times (5–240 min). Uranium ion removal initially increased rapidly within the first 10 min and slowly after, between 10 and 60 min, that till the equilibrium was achieved within 180 min, with no further increase after 180 min. (Fig. 4). Initially, all binding sites on O/AC and N/O/AC are vacant and so available for uranium ions to interact (the first 10 min) besides the higher ratio of uranium ions to the active sites. With the progress, the reaction between the O/AC and N/O/AC and uranium ion leads to decreasing of the vacant binding sites, hence the adsorption was reduced.

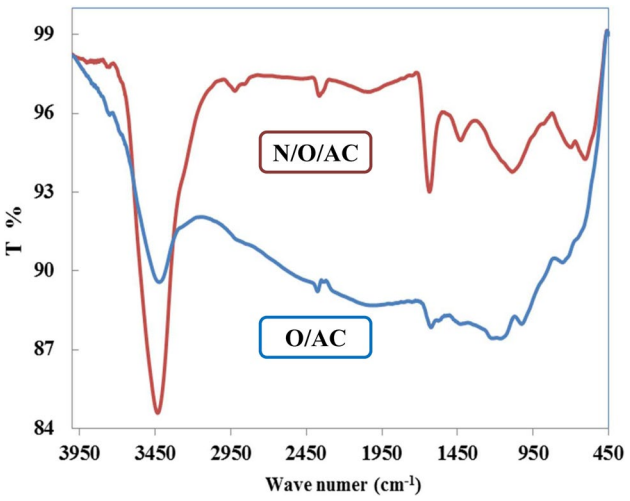

Fig. 2 FT-IR of O/AC and N/O/AC

The appropriateness of the five dynamic models was clarified to depict the U(VI) removal by O/AC and N/O/AC. Using the Lagergren or pseudo-first-order equation, kinetic analysis was carried out. The earliest model of the rate of liquid/solid-phase adsorption was introduced by Lagergren based on the relation between the logarithmic values of adsorption potential at equilibrium (q_e) and deferred time (q_t) with time (t) (Tag El-Din et al. 2018a).

$$\log\left(q_e - q_t\right) = \log\left(q_1\right) - \frac{k_1}{2.303}t, \tag{6}$$

q_1, theoretical adsorption capacity according to Lagergren, and k_1, Lagergren constant of the Lagergren equation, were quantified from the log (q_e-q_t) vs (t) plot (Fig. 5).

The pseudo-second-order equation is focused on the relation between the values of contact time/ the adsorption capacity at different times with the contact time (Eq. 8) (Tag El-Din et al. 2018a; Torrik et al. 2019).

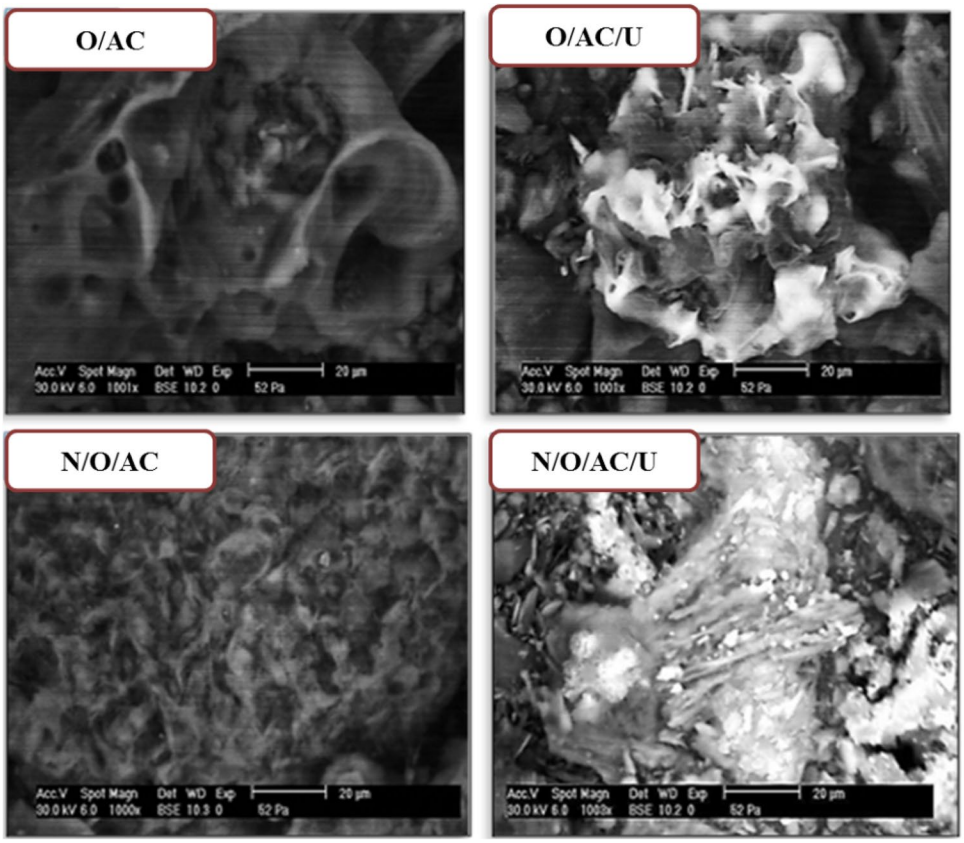

Fig. 3 SEM images of O/AC, O/AC/U(VI), N/O/AC, and N/O/AC/U(VI)

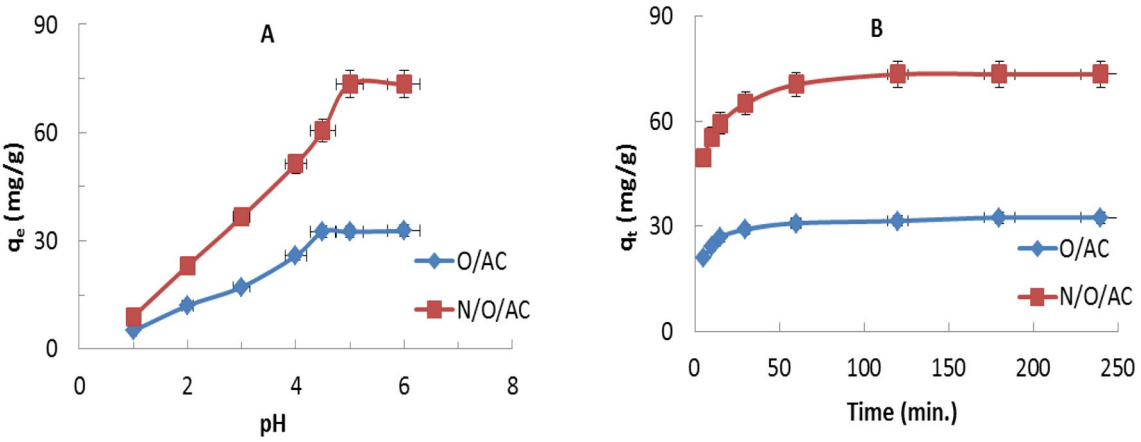

Fig. 4 Effect of solution pH (**a**) contact time (**b**) on U(VI) removal by O/AC and N/O/AC

$$\frac{t}{q_t} = \frac{1}{k_2 q_2^2} + \frac{1}{q_e} t, \tag{7}$$

q_2 (theoretical adsorption capacity$_)$ and k_2 (rate constant of the pseudo-second-order) were quantified from the drawn relation of (t/q_t) vs. (t) (Fig. 5 and Table 2). There was coherence with laboratory results in pseudo-second-order model outcomes.

Elovich or Roginsky–Zeldovich approach was included to identify if the rate of adsorption of uranium on adsorbent decreases exponentially with an increase of uranium adsorbed according to the Elovich equation as follows: (Atia et al. 2019).

$$q_t = \frac{1}{\beta}\ln(\alpha\beta) + \frac{1}{\beta}\ln(t). \tag{8}$$

The initial adsorption rate (α) and the adsorption constant (β) were calculated from Elovich plots (q_t vs. ln t). The extreme differences between the calculated α values and the experimental q_e (Fig. 5 and Table 2) indicate that the Elovich model does not describe the adsorption of uranium ions by O/AC and N/O/AC.

The time-dependent data were used to investigate whether liquid film diffusion and intra-particle kinetics played significant roles in uranium adsorption onto O/AC and N/O/AC. To test the essence of the boundary layer in the adsorption reaction, time data were treated by the liquid film diffusion model Eq. 9 (Abu El-Soad et al. 2019).

$$\log(1 - F) = -\frac{K_{fd}}{2.303} t, \tag{9}$$

where K_{fd} is the film diffusion rate constant (min^{-1}) and F is a constant equals the value of q_t/q_e. When the plotting of log (1-F) versus (t) gives a line with zero intercept, it increases the chance that the film diffusion is slow. The rate constant for liquid film diffusion (K_{fd}) is 0.03 and 0.04 for (O/AC) and (N/O/AC), respectively. For the adsorption time data of U(VI) ions, the constructed relation of log (1−F) versus time, t (Fig. 5) gave a non-zero intercept (Table 2). It indicates the futility of film diffusion in explaining the interaction.

Weber–Morris or Intra-particle diffusion model suggests that adsorption varies almost proportionally with ($t1^{/2}$) rather than with the (t), Eq. 10 (Abu El-Soad et al. 2019).

$$q_t = K_{ip} t^{0.5} + I \tag{10}$$

The kinetic parameters and data of the Weber-Morris model were detected from the relation between q_e versus $t^{0.5}$ (Fig. 5 and Table 2). The smaller values of I and K_{ip} almost equal to zero (higher R^2 values) indicate the intra-particle diffusion as a rate-controlling step.

The Bangham model suggested that the diffusion of the adsorbate into the pores of the adsorbent controls the reaction**.** The adsorption data were applied to the Bangham model according to Eq. 11 (Abd El-Magied et al. 2016, 2018).

$$\text{loglog}\left(\frac{C_i}{C_i - mq_t}\right) = \log\left(\frac{mK_b}{2.303V}\right) + \alpha\log(t). \tag{11}$$

where m, α, and K_b are Bangham constants and adsorbent, s weight/solution volume, (g/L), respectively. By application of Bangham model on U(VI) ions adsorption onto the used activated carbons, the plots of loglog $\left(\frac{C_i}{C_i - mq_t}\right)$ vs. log (t) give straight lines with high R^2 values. This study demonstrates also that uptake is dictated by pore-diffusion controlled.

.

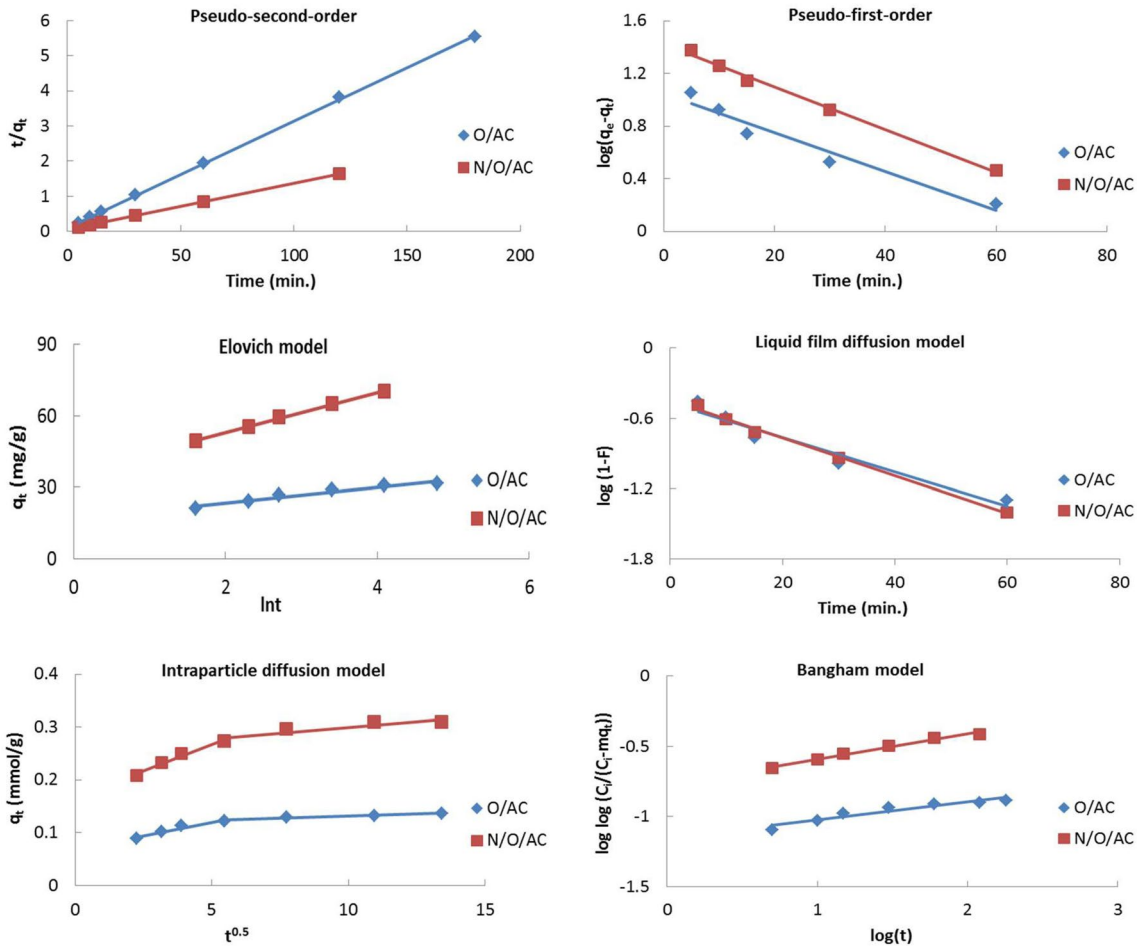

Fig. 5 The used kinetics models for U(VI) adsorption onto O/AC and N/O/AC

Effect of Initial U(VI) Ion Concentration at Different Temperature

The effect of initial U(VI) ion concentration and the adsorption capacity at the 25 °C showed a mutual increase between the two variants till reaching the plateau at which the maximum uptake values by O/AC and N/O/AC (due to increasing the availability of uranium ions for adsorption sites). The improvement of the adsorption process with increasing the initial U(VI) ions concentration is reasonably explained by decreasing the resistance to mass transfer from the solution to sorbents solid phases.

The effect of operating temperature variations (298, 303, 313, and 323) on the uranium sorption was studied (Fig. 6). The results revealed a relative increase in the sorption with an increase in temperature. Higher temperatures increased the mobility of the uranium ions, which enhanced the penetration of it inside the pores of the O/AC and N/O/AC and increase diffusion through the internal and external boundary layer of the O/AC and N/O/AC beads.

Adsorption Isotherms

Langmuir assumes that the adsorption can be regarded as a reversible process between adsorbent (Uranium) and adsorbate (O/AC and N/O/AC), Eq. 12 (Sadeek et al. 2014; Nazari et al. 2020).

$$\frac{C_e}{q_e} = \frac{C_e}{Q_{max}} + \frac{1}{K_L Q_{max}} \tag{12}$$

The Langmuir adsorption capacity (Q_{max}) and binding constant (K_L) were obtained from Fig. 7**.** Plotting of (C_e/q_e) versus (C_e) shows high correlation coefficients (R_2). The Q_{max} (corresponding to complete monolayer sorption at different temperatures) agrees with the experimentally obtained. The increase in values of K_L and Q_{max} with the temperature may be due to enhancement binding between U(VI) ions and O/AC and N/O/AC at higher temperatures.

Table 2 Kinetic parameters of different models used to fit the U(VI) adsorption process

Kinetic model	Parameters	O/AC	N/O/AC
Experimental	q_e (mg/g)	32.45	73.41
Pseudo-first-order kinetics	q_{1st}, (mg/g)	11.0204	26.3572
	k_1, (min^{-1})	0.0338	0.0370
	R^2	0.9486	0.9948
Pseudo-second-order kinetics	q_{2nd}, (mg/g)	32.8947	75.1879
	K_2, (g/mg.min.)	0.0084	0.0035
	R^2	0.9998	0.9997
Elovich kinetic	β (g/mg)	0.3004	0.1183
	α (mg/g.min)	514.613	607.8564
	R^2	0.937	0.999
Intraparticle diffusion	K_{ip}, (mg/g.$min^{0.5}$)	0.0103	0.0197
	I	0.0683	0.1683
	R^2	0.9402	0.9755
Liquid film diffusion	K_{fd}	0.0338	0.0370
	R^2	0.9486	0.9948
Bangham kinetic	K_b (mL/g/L)	32.2495	77.6647
	A	0.1287	0.18
	R^2	0.914	0.9841

The suitability of the O/AC and N/O/AC towards uranium ions can be tested from the values of the separation factor constant (R_L) using Eq. (13) (Abd El-Magied et al. 2016).

$$R_L = \frac{1}{1 + K_L C_o}, \tag{13}$$

where C_o is the initial concentration of U(VI) ions (mM). The calculated separation factors (R_L) for the O/AC and N/O/AC ranged from 0.02 to 0.45 (Table 3). These R_L values point to the high favorability of the uranium sorption process (Fig. 7).

Freundlich isotherm assumes that the sorption process is non-ideal, reversible and multilayer (Sadeek et al. 2014; Demir Delil et al. 2019). The adsorption data of U(VI) ions at 25^0C were tested according to the Freundlich model (Eq. 14).

$$\log q_e = \log K_F + \frac{\log C_e}{n}. \tag{14}$$

The values of Freundlich parameters (relative sorption capacity (K_F) and intensity of sorption (n)) were calculated (Table 3). The Freundlich plots gave a slope less than 1 refers to a suitable adsorption process of U(VI) under the concentration spectrum investigated, Fig. 7. However, the diversity of theoretical adsorption capacities calculated from Freundlich and the experimental one confirms Freundlich's failure to apply to U(VI) adsorption being studied.

The Temkin isotherm, like Freundlich, is among the earliest reported isotherms and assumes adsorption heat is reduced by increasing coverage linearly. The Temkin isotherm can be described by the following equations (Abd El-Magied et al. 2016).

$$q_e = \frac{RT}{b} \ln A_T + \frac{RT}{b} \ln C_e, \tag{15}$$

$$B = \frac{RT}{b},$$

$$q_e = B \ln A_T + B \ln C_e. \tag{16}$$

Temkin binding constant (A_T), isotherm constant (b), and heat of sorption (B) were calculated from Temkin plots (Fig. 7) and reported in Table 3. The estimated β values of O/AC and N/O/AC were 6.6 and 7 kJ/mol, respectively. These data indicate a physical-sorption process; the estimated β values are ≤ 20 kJ/mol.

Dubinin–Radushkevich isotherm model estimates the energy of adsorption to verify the adsorption process as physical sorption or chemisorption. The adsorption data were treated with the Dubinin–Radushkevich model according to Eq. 17 (Abu El-Soad et al. 2019).

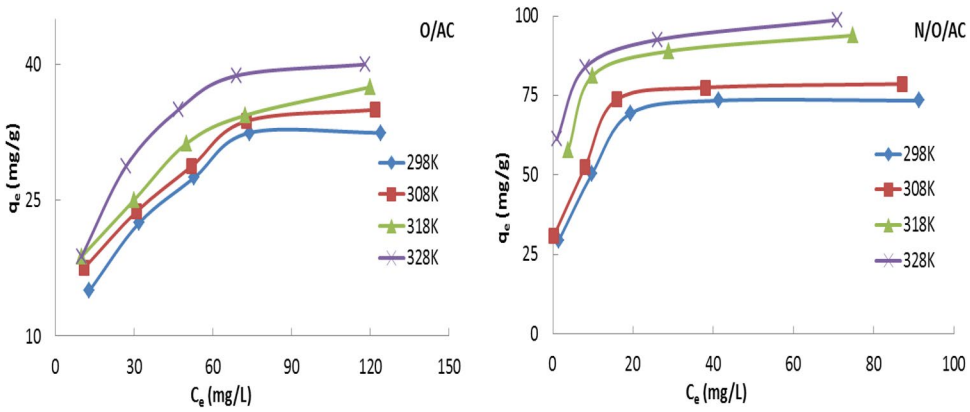

Fig. 6 Effect of U(VI) concentration at different temperatures on the adsorption process

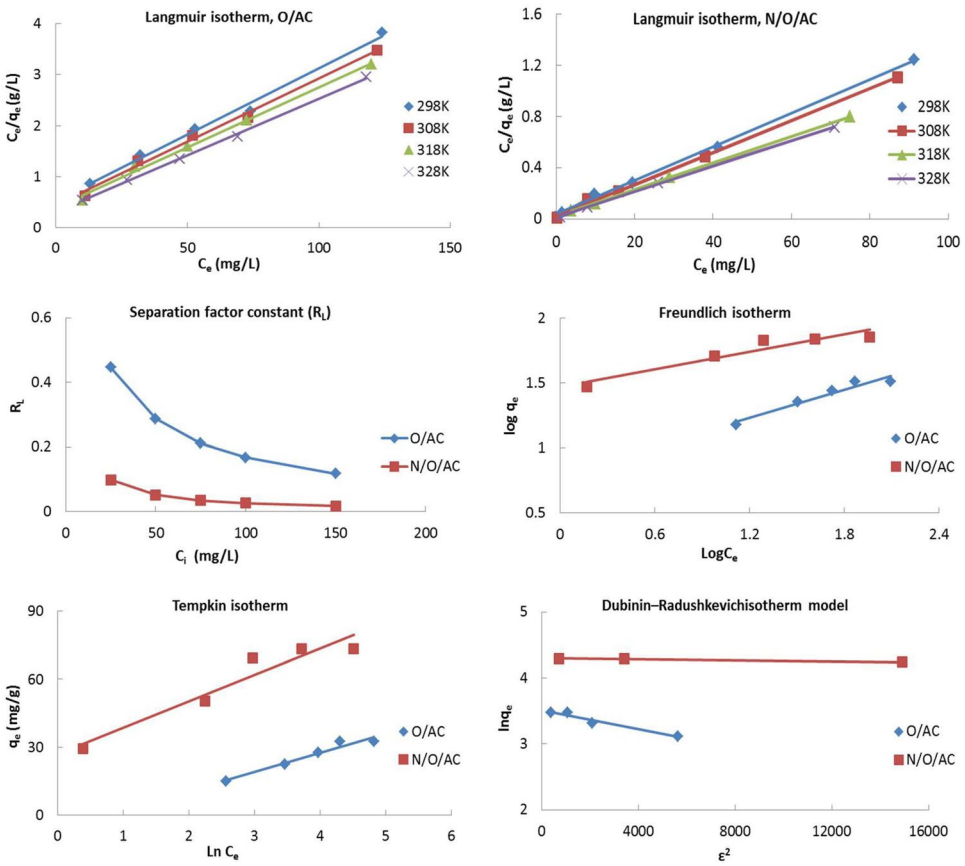

Fig. 7 Adsorption isotherms models for U(VI) removal by O/AC and N/O/AC

$$\ln q_e = \ln q_s - K_{ad}\varepsilon^2, \text{ where } \varepsilon = RT\ln\left[1 + \frac{1}{C_e}\right]. \quad (17)$$

K_{ad} and ε are constants of the D–R model. Plotting D–R plot (Fig. 7) gave a straight line with slope and intercepts equal to β and $\ln q_D$, respectively. The apparent energy ($E = KJ/mol^2$) could be evaluated when using K_D values using Eq. 18.

$$E = \left[\frac{1}{\sqrt{2K_D}}\right]. \quad (18)$$

The calculated value of the adsorption mean free energy was found to be 8.4515 and 11.1803 kJ/mol for O/AC and N/O/AC, respectively (Table 3). These results refer to the physical nature of the adsorption process.

Solid/Liquid Ratio

Under fixed conditions of U(VI) concentration (100 mg/L), operating temperature (25 °C), and adsorption solution (25 mL), the adsorbent dose impact on the capability of adsorption was examined (between 10 and 200 mg), Fig. 8.

Table 3 Adsorption isotherms of U(VI) ions by O/AC and N/O/AC

Isotherms model	Parameters	O/AC	N/O/AC	Temp
Experimental	q_e (mg/g)	32.45	73.41	298 K
Langmuir	$Q_{max,}$ (mg/g)	38.4615	76.336	298 K
		40.1606	81.967	308 K
		42.3728	97.087	318 K
		45.2488	100	328 K
	K_L (L/mg)	0.0496	0.3530	298 K
		0.0568	0.5232	308 K
		0.0598	0.6687	318 K
		0.0715	0.7407	328 K
	R_L	0.446	0.102	298 K
	R^2	0.9923	0.9985	
Freundlich	$K_{F,}$ (mg/g)	6.1887	28.973	298 K
	N	2.7397	4.199	
	R^2	0.9451	0.9079	
D-R	$q_{D,}$ (mg/g)	33.5621	74.0025	298 K
	K_{ad} mol^2/kJ^2	0.000007	0.000004	
	E, (kJ/mol)	8.4515	11.1803	
	R^2	0.9517	0.9681	
Temkin	β (kJ/mol)	6.620	7.011	298 K
	A_T (L/g)	0.395	45.925	
	b	374.24	353.374	
	R^2	0.9543	0.916	

The results (Fig. 8) indicated that the maximum uranium removal efficiency (%) was 82 and 99% for O/AC and N/O/AC at a dose of 4 mg/mL. This is reasonably ascribed to the increasing of the O/AC and N/O/AC surface area and the more available adsorption sites.

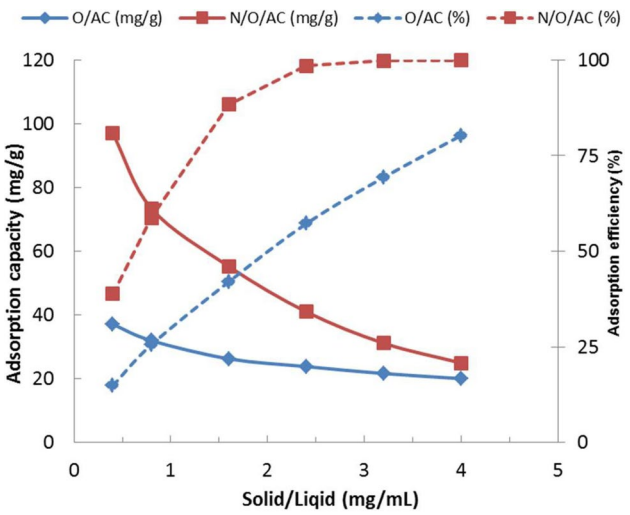

Fig. 8 Adsorption dose effects on adsorption performance

Thermodynamic Parameters

The values of K_L at the different temperatures from the Langmuir model were used for the evaluations of thermodynamic parameters, and calculate the enthalpy change (ΔH^o) and entropy change (ΔS^o) using Van't Hoff equation, Fig. S4 (SI), (Sadeek et al. 2014; Tony and lin 2021; de Sá et al. 2021).

$$\ln K_L = \frac{\Delta S^o}{R} - \frac{\Delta H^o}{RT}. \quad (19)$$

The Gibbs free energy, ΔG° was calculated from the obtained values of ΔH^o and ΔS^o using Eq. 20.

$$\Delta G^o = \Delta H^o - T\Delta S^o. \quad (20)$$

The calculated thermodynamic parameters ΔH^o, ΔS^o, and ΔG^o are reported in Table 4. The negative values of ΔG^o reflect the high affinity of uranium to O/AC and N/O/AC as well as the spontaneity of reaction. Additionally, increasing the negativity of the ΔG^o values with the temperature increasing reflects the proportionality between the spontaneity of the sorption process and the applied temperature that means the more favorability of uranium sorption with elevated temperature. In a similar meaning, the positive value of ΔH^o confirms the endothermic nature of the U(VI) ions adsorption process and that the intensity of sorption is enhanced at higher temperatures.

Adsorbent Regeneration

The regeneration of adsorbents offers various advantages: cost-efficiency, limited disposal cost, reduction of environmental hazards, and metals recovery. Regeneration of O/AC and N/O/AC from uranium was studied using a batch system, Table 5. Among all mediums, 0.25 M HNO_3 was found to be good enough for desorbing the adsorbed U(VI) from the adsorbents (96.8%).

Application on Contaminated Groundwater

In southwestern Sinai, Egypt, several water wells are used for drinking and other human activities. Occasionally, this groundwater records a higher concentration of uranium and other heavy metals than the permissible levels, due to aqueous/rock interaction as well as the rain effect that leaches some metals from surrounding rocks then penetrates to the underground as a feeding source for the water wells.

Four water wells (Well-1, Well-2, Well-Zeid, and Well-Oda) in the Wadi Naseib area, southwestern Sinai, Fig. S5, were sampled to verify the target of this study. Wadi Nasieb area is considered the drainage base of an important radioactive mineralized area known as Gabal Allouga and is covered by different rocks of the Precambrian and Paleozoic ages.

The Precambrian basement rocks consist of diorite and granodiorite with extrusive acidic dykes, are mainly exposed in the east and south of Wadi Naseib. The exposed Paleozoic rocks in the Wadi Naseib area are classified into two types: mineralized and non-mineralized sediments. Gabal Allouga's main radioactive field is related to the presence of certain secondary minerals in uranium.

Additionally, the sedimentary cover exposed on both sides (east and west) of Wadi Naseib consists of Cambrian sandstone, siltstone, shale, Lower Carboniferous dolomite, marl, and black shale (Um Bogma Formation) and sandstone and gray shale of Abu Thora Formation. The dolomite, marl, and black shale of Um Bogma Formation represent high-grade uraniferous rocks. The flash floods in this area usually starting from Gabal Allouga at the southern extreme of the map and have their course to the East and then to the North till Wadi El Seih (outside the map).

The content of four water wells in the Wadi Naseib area was identified and illustrated in Table 6. Most of those constituents are derived from the surrounding rocks by rainfall leaching and are especially uranium and other heavy metals.

The groundwater from the Wadi Naseib area, southwestern Sinai, Egypt was tested for pollutant removal by the direct interaction with O/AC and N/O/AC. The adsorption process from the contaminated groundwater was carried out,

Table 4 Thermodynamic parameters

Adsorbents	Temp (Kelvin)	Thermodynamic parameters			
		ΔH^o (kJ/mol)	ΔS^o (KJ/mol.K)	$T\Delta S^o$ (kJ/mol)	ΔG^o (kJ/mol)
O/AC	298	9.293	0.109	32.518	– 23.225
	308			33.609	– 24.3159
	318			34.701	– 25.407
	328			35.7918	– 26.498
N/O/AC	298	19.49	0.1625	47.444	– 27.848
	308			48.830	– 29.332
	318			50.422	– 30.949
	328			52.008	– 32.545

Table 7. The uranium and other metals concentrations are below these levels when compared to reference limits of the same metals in drinking water (Nda et al. 2011).

The non-treated groundwater samples of well-1 and well-2, as well as the treated sample of well-1 by the adsorbents, were subjected to the activity–concentrations analysis using the High-Purity Germanium (HPGe) ɣ-ray spectrometer, Table 8.

Based on the resulted radionuclide types and their activity concentrations (Bq/L), Table 8, more than one issue should be elaborated:

(1) The approximate complete similarity between the chemically determined uranium in well-1 and well-2 (1.8 and 1.1 mg/L) and the calculated values (after conversion from the Bq l^{-1} to the ppm unit) from the activity concentration (1.788 and 1.03 mg/L);
(2) The complete disappearance of the uranium, and its daughters, from the samples after the treatment by O/AC and N/O/AC;
(3) Finally, the absence of ^{226}Ra activity that could point to the recent age of the present uranium, and the fourth is that ^{232}Th activity concentration is expressed by the average activities of the peaks of ^{228}Ac and ^{208}Tl.

^{232}Th and ^{238}U decay radionuclides are a source of exposure to external and internal radiation. Internal exposure occurs via the inner breath of radon gas and external exposition occurs via the flow from radiation sources into gamma rays. From a natural risk standpoint, the public exposure dose limits must be known and human exposure to natural radiation sources estimated (El-Taher and Makhluf 2010; Tufail 2012; Alaboodi et al. 2020).

Table 5 Regeneration of O/AC and N/O/AC

Desorbing agents	Desorption % of Uranium			
	O/AC	N/O/AC	HNO3 (M)	N/O/AC
H_2O	0.7	0.6	0.05	51.5
NaOH (0.1 M)	1.6	1.8	0.1	68.6
HCl (0.1 M)	31.7	34.1	0.15	71.3
HNO_3 (0.1 M)	65.3	68.5	0.2	82.5
H_2SO_4 (0.1 M)	27.5	31.9	0.25	96.8

Radium equivalent activity ($Ra_{eq,}$ Bq/L): Ra_{eq} is used to represent radioactive hazards associated with ^{226}Ra, ^{232} K, and ^{232}Th into a single quantity using their activity concentrations (A) by Eq. 21. It is supposed to be equal gamma-ray dose are produced from 130 Bq/L of ^{40} K, 7 Bq/L of ^{232}Th or 10 Bq/L of ^{226} Ra, and Raeq must not exceed the 370 Bq/L limit.

$$Ra_{eq}\left(Bq/L\right) = A_{Ra} + 0.0769A_K + 1.4286A_{Th}. \quad (21)$$

Absorbed dose rate (D, nGy/h): D (nGy/h) used for the description of the terrestrial radiation for distribution (regular) of ^{40} K, ^{232}Th and ^{226}Ra. D, nGy/h, can be determined with Eq. 22:

$$D(nGy/h) = 0.462A_{Ra} + 0.0417A_K + 0.604A_{Th}. \quad (22)$$

Internal radiation hazard index (H_{in}): H_{in} determines the internal exposure caused by Rn (radon) and daughter of Rn (Eq. 23). To avoid the radiation danger, the values of the H_{in} must be < unity

Table 6 Chemical analyses (mg/L) of water wells samples

Elements	Concentration (mg/L)			
	Well -1	Well -2	Well-Oda	Well-Zeid
pH	7.5	7.2	7.1	7.3
TDS	2810	1450	950	760
Ca^{2+}	343	123	98	86
Mg^{2+}	277	110	96.5	84
Na^+	314	185	130	118
K^+	35	9.5	7	8
SO_4^{2-}	452	480	318	290
CO_3^{2-}	510	185	105	77
Cl^-	370	165	74	78
U	1.8	1.1	0.4	0.1
Ni	17.6	2.4	1.07	0.9
Cu	0.018	0.007	0.015	0.018
Co	0.022	0.006	0.003	0.005
Cr	0.004	0.001	0.01	0.005
As	0.017	0.011	0.005	0.003
Cd	0.008	0.001	0.009	0.006
Pb	0.091	0.003	< 0.001	< 0.001
Fe	2.067	1.004	0.45	0.1

Table 7 Analyses of groundwater samples after treating them with the absorbent

Adsorbent	Element	Permissible levels, mg/L	Well-1	Well-2	Well-Oda	Well-Zeid
O/AC	U	0.03–0.015	0.013	0.008	< 0.001	< 0.001
	Ni	0.1	0.1	0.02	< 0.001	< 0.001
	Cu	1.0	0.01	< 0.001	< 0.001	< 0.001
	Co	0.002	0.01	< 0.001	< 0.001	< 0.001
	Cr	0.1	< 0.001	< 0.001	< 0.001	< 0.001
	As	0.01	0.01	0.001	< 0.001	< 0.001
	Cd	0.005	< 0.001	< 0.001	< 0.001	< 0.001
	Pb	0.015	0.010	< 0.001	< 0.001	< 0.001
	Fe	0.3	0.20	0.10	< 0.001	< 0.001
N/O/AC	U	0.03–0.015	< 0.001	< 0.001	< 0.001	< 0.001
	Ni	0.1	< 0.001	< 0.001	< 0.001	< 0.001
	Cu	1.0	< 0.001	< 0.001	< 0.001	< 0.001
	Co	0.002	< 0.001	< 0.001	< 0.001	< 0.001
	Cr	0.1	< 0.001	< 0.001	< 0.001	< 0.001
	As	0.01	< 0.001	< 0.001	< 0.001	< 0.001
	Cd	0.005	< 0.001	< 0.001	< 0.001	< 0.001
	Pb	0.015	0.005	< 0.001	< 0.001	< 0.001
	Fe	0.3	0.02	< 0.001	< 0.001	< 0.001

$$H_{in} = \frac{A_{Ra}}{185} + \frac{A_K}{4810} + \frac{A_{Th}}{259}. \quad (23)$$

External hazard radiation index (H_{ex}): H_{ex} (Eq. 24) is used to quantify the hazard of the natural gamma (γ) radiation (results from γ emission from natural radionuclides in the environment). To keep this hazard insignificant, the H_{ex} needs to be < unit (H_{ex}'s highest value = 1)

$$H_{ex} = \frac{A_{Ra}}{370} + \frac{A_K}{4810} + \frac{A_{Th}}{259} \leq 1. \quad (24)$$

Representative level index or gamma-index (I_γ): I_γ represents the γ radiation hazard associated with natural γ. The value of Iγ must be lower than unity(Eq. 25).

$$I_\gamma = \frac{A_{Ra}}{300} + \frac{A_K}{3000} + \frac{A_{Th}}{200}. \quad (25)$$

Alpha radiation index (I_α): I_α represents the alpha radiation hazard associated with natural alpha according to Eq. 26.

$$I_\alpha = \frac{A_{Ra}}{200}. \quad (26)$$

The environmental radioactive indices were calculated for some studied water samples and illustrated in Table 9. Referring to the values of the calculated hazards indices, all are in quite safe limits according to the recommended values by the international and specialized agencies. The recommended value for the Ra_{eq} is 370 Bq/L, the global average value of D parameter ranges between 100 and 200 nGy/h, while the unity is the recommended safe value for H_{int}, $H_{ext,}$ and Iγ indices(El-Taher and Makhluf 2010; Tufail 2012; Alaboodi et al. 2020).

From the above illustration, it can be demonstrated that there are no environmental hazards that could affect the surrounding environment or people by the emitted gamma-ray amounts from the dissolved radionuclides in the groundwater even before the treatment process. The main risk is connected with the emitted alpha particles from the uranium when it goes into the human body with the drinking water. Anyhow, the positive effect of the used adsorbents (on the removal or minimizing the radioactive daughters consequently reduction of the hazard indices values) should be noted, this effect will be very helpful and effective with the old-age uranium concentrations.

Conclusion

The current work aimed to reduce uranium concentration in groundwater wells of the Wadi Naseib area, southwestern Sinai, Egypt to their safe limits of concentration which represent a vital issue for human health. To conduct this goal, low-cost and high-efficient activated carbons, as adsorbents, were prepared from graphite, as raw materials. The activated carbons were obtained through the steam pyrolysis of the raw materials, while the modified forms were prepared by oxidation of adsorbents using HNO_3 acid followed by treatment with N'-[2-[2-(2-Aminoethylamino)ethylamino]

Table 8 The activity concentrations of radionuclide in the groundwater sample

Activity	Before treatment			
	Well -1		Well-2	
Radionuclide	Activity, Bq/L	Content	Activity, Bq/L	Content
^{238}U-series				
^{238}U	22.18 ± 2.62	1.79 ± 0.11 mg/L	12.75 ± 0.79	1.03 ± 0.06 mg/L
^{234}U	78.72 ± 4.73		42.21 ± 3.17	
^{230}Th	18.86 ± 6.32		10.36 ± 6.02	
^{226}Ra	——- ± ——-			
^{214}Pb	——- ± ——			
^{214}Bi	——- ± ——-			
^{210}Pb	——- ± ——-			
^{235}U	1.02 ± 0.07	0.013×10^{-4} mg/L	0.45 ± 0.110	0.006 ± 0.001 mg/L
^{232}Th-series				
^{228}Ac	1.38 ± 0.13		1.305 ± 0.051	
^{208}Tl	1.17 ± 0.04		1.009 ± 0.032	
Average	1.27 ± 0.08	0.32 ± 0.02 mg/L	1.157 ± 0.042	0.279 ± 0.01 mg/L
^{40} K	21.83 ± 2.14	0.07 ± 0.007 (%)	19.6 ± 2.340	0.063 ± 0.007%
Activity	After treatment			
	Well-1			
	After (O/AC)		After (N/O/AC)	
Radionuclide	Activity, Bq/L	Content	Activity, Bq/L	Content
^{238}U-series				
^{238}U	0.90 ± 0.06	0.07 ± 0.01 mg/L	——-	——-
^{234}U	——-		——-	——-
^{230}Th	——-		——-	——-
^{226}Ra	——-		——-	——-
^{214}Pb	——-		——-	——-
^{214}Bi	——-		——-	——-
^{210}Pb	——-		——-	——-
^{235}U	——-		——-	——-
^{232}Th-series				
^{228}Ac	1.27 ± 0.05		1.23 ± 0.037	
^{208}Tl	1.08 ± 0.003		1.04 ± 0.036	
Average	1.17 ± 0.03	0.291 ± 0.004 mg/L	1.13 ± 0.037	0.281 ± 0.914 mg/L
^{40} K	5.57 ± 0.04	0.018 ± 0.0004%	3.44 ± 0.996	0.011 ± 0.0003%

ethyl]ethane-1,2-diamine (Tepa). The different characteristics of the active carbon samples such as the surface area, ash content, functional groups and the elemental analysis were identified. To conduct the optimum controlling factors that affect the adsorption process, several synthetic solutions of various concentrations of uranium were prepared and tested with the prepared activated carbon samples. The variables examined included; solution pH, solid–liquid contact time, initial concentration of the target hazards, amount of the adsorbent, and operational temperature. Also, several isotherm models (Langmuir, Freundlich, Dubinin–Radushkevich, and Temkin) were applied to test the equilibrium relationship between the solid- and liquid-phase concentration of the contaminants. Also, the Pseudo-first-order, Pseudo-second-order, intra-particle diffusion, Elovich, Liquid film diffusion, and Bangham kinetic models were used to clarify the adsorption mechanism. Desorption of the adsorbate, for adsorbent reusing, was executed for the loaded activated carbon samples using different chemical agents (NaOH, HCl, HNO_3, and H_2SO_4). In an application step, the achievable

Table 9 The calculated hazards indices of some studied water samples

		$Ra_{eq}(Bql^{-1})$	D (nGy h^{-1})	H_{int}	H_{ext}	Iγ	Iα
Before treatment	Well-1	3.50	1.680	0.009	0.009	0.014	–
	Well-2	3.16	1.52	0.008	0.008	0.012	–
After treatment (Well-1)	O/AC	2.11	0.94	0.006	0.006	0.008	–
	N/O/AC	1.88	0.83	0.005	0.005	0.007	–

optimum conditions were applied to the groundwater samples. The prepared activated carbon and their modified form provided low-cost and high-efficient adsorbents that can be used successfully in removing hazardous elements. The concerned groundwater should be treated before releasing it to domestic uses. The amino-adsorbent is preferred due to its enhanced removal efficiency regarding the hazardous pollutants. Finally, the current work is regarded as an effective contribution to the effects delivered to the management of environmental pollution.

Declarations

Conflicts of interest The authors declare no conflict of interest.

References

Abd El-Magied MO (2016) Sorption of uranium ions from their aqueous solution by resins containing nanomagnetite particles. J Eng. https://doi.org/10.1155/2016/7214348

Abd El-Magied MO, Hassan AM, Gad HMH, Mohammaden TF, Youssef MAM (2017) Removal of nickel (II) ions from aqueous solutions using modified activated carbon: a kinetic and equilibrium study. J Dispersion Sci Technol 39:862–873. https://doi.org/10.1080/01932691.2017.1402337

Abd El-Magied MO, Mansour A, Alsayed FA, Atrees MS, Abd Eldayem S (2018) Biosorption of beryllium from aqueous solutions onto modified chitosan resin: Equilibrium, kinetic and thermodynamic study. J Dispersion Sci Technol 39:1597–1605. https://doi.org/10.1080/01932691.2018.1452757

Abu El-Soad AM, Abd El-Magied MO, Kovaleva EG, Lazzara G (2019) Synthesis and characterization of modified sulfonated chitosan for beryllium recovery. Int J Biol Macromol 139:153–160. https://doi.org/10.1016/j.ijbiomac.2019.07.162

Alaboodi A, Kadhim N, Abojassim A, Baqir HA (2020) Radiological hazards due to natural radioactivity and radon concentrations in water samples at Al-Hurrah city, Iraq. Int J Radiat Res 18:1–11

Alahabadi A, Singh P, Raizada P, Anastopoulos I, Sivamani S, Dotto GL, Landarani M, Ivanets A, Kyzas GZ, Hosseini-Bandegharaei A (2020) Activated carbon from wood wastes for the removal of uranium and thorium ions through modification with mineral acid. Colloids Surf A 607:125516. https://doi.org/10.1016/j.colsurfa.2020.125516

Amini A, Khajeh M, Oveisi AR, Daliran S, Ghaffari-Moghaddam M, Delarami HS (2021) A porous multifunctional and magnetic layered graphene oxide/3D mesoporous MOF nanocomposite for rapid adsorption of uranium(VI) from aqueous solutions. J Ind Eng Chem 93:322–332. https://doi.org/10.1016/j.jiec.2020.10.008

Atia BM, Gado MA, Abd El-Magied MO, Elshehy EA (2019) Highly efficient extraction of uranyl ions from aqueous solutions using multi-chelators functionalized graphene oxide. Sep Sci Technol 55:2746–2757. https://doi.org/10.1080/01496395.2019.1650769

Bai J, Ma X, Yan H, Zhu J, Wang K, Wang J (2020) A novel functional porous organic polymer for the removal of uranium from wastewater. Micropor Mesopor Mat 306:110441. https://doi.org/10.1016/j.micromeso.2020.110441

Cheremisinoff NP (2002) Handbook of water and wastewater treatment technologies. Butterworth-Heinemann, Oxford

Coates J (2000) Interpretation of infrared spectra, a practical approach. In: R.A. Meyers (Ed) Encyclopedia of analytical chemistry. Wiley, Chichester.

Delil AD, Gülçiçek O, Gören N (2019) optimization of adsorption for the removal of cadmium from aqueous solution using Turkish coffee grounds. Int J Environ Res 13:861–878. https://doi.org/10.1007/s41742-019-00224-6

Donia AM, Atia AA, Daher AM, Desouky OA, EA. Elshehy EA, (2011a) Selective separation of Th(IV) from its solutions using amine modified silica gel produced from leached zircon. J Radioanal Nucl Chem 290:297–306. https://doi.org/10.1007/s10967-011-1162-3

Donia AM, Atia AA, Daher AM, Desouky OA, Elshehy EA (2011b) Synthesis of amine/thiol magnetic resin and study of its interaction with Zr(IV) and Hf(IV) ions in their aqueous solutions. J Dispersion Sci Technol 32:634–641. https://doi.org/10.1080/01932691003799860

El-Said WA, El-Khouly ME, Ali MH, Rashad RT, Elshehy EA, Al-Bogami AS (2018) Synthesis of mesoporous silica-polymer composite for the chloridazon pesticide removal from aqueous media. J Environ Chem Eng 6:2214–2221. https://doi.org/10.1016/j.jece.2018.03.027

Elshehy EA (2017) Removal of uranium ions from liquid radioactive waste using modified aluminosilica. Sep Sci Technol 52:1852–1861. https://doi.org/10.1080/01496395.2017.1297829

El-Taher A, Makhluf S (2010) Natural radioactivity levels in phosphate fertilizer and its environmental implications in Assuit governorate, Upper Egypt. Indian J Pure Appl Phys 48:697–702

Friedlander G, Kennedy JW, Macias ES, Miller JM (1981) Nuclear and radiochemistry. Wiley, New York

Leiner de Sá M, Nobre FX, Silva LS, Sousa GS, Takeno ML, Júnior EAA, Elias de Matos JM, Chaves de Santos MRM (2021) Preparation of new h-MoO_3 rod-like microcrystals for effective removal of cationic dye in aqueous solution. Int J Environ Res 15:105–124. https://doi.org/10.1007/s41742-020-00301-1

Loveland WD, Morrissey DJ, Seaborg GT (2006) Modern nuclear chemistry. Wiley, New York

Mahmoud ME, Fekry NA, Abdelfattah AM (2020) Removal of uranium (VI) from water by the action of microwave-rapid green synthesized carbon quantum dots from starch-water system and supported onto polymeric matrix. J Hazard Mater 397:122770. https://doi.org/10.1016/j.jhazmat.2020.122770

Marczenko Z (1976) Separation and spectrophotometric determination of elements. Ellis Harwood Limited, Chichester

Mokhine ND, Mathuthu M, Stassen E (2020) Recovery of uranium from residue generated during Mo-99 production, using organic solvent extraction. Phys Chem Earth Parts A/B/C 15:102822. https://doi.org/10.1016/j.pce.2019.102822

Nada AA, Talaat SM, Abd El Maksoud TM, ElAassy IE, El Galy MM, El Feky MG, Ibrahim EM (2011) Effect of flash flood in the distribution of radionuclides of groundwater and its environmental impacts, Wadi Naseib, Southwestern Sinai. Egypt Isot Radiat Rese 43:1575–1593

Nazari A, Nakhaei M, Yari AR (2021) Arsenic adsorption by TiO_2 nanoparticles under conditions similar to groundwater: batch and column studies. Int J Environ Res 15:79–91. https://doi.org/10.1007/s41742-020-00298-7

Sadeek SA, Abd El- Magied MO, El-Sayed MA, Amine MM (2014) Selective solid-phase extraction of U(VI) by amine functionalized glycidyl methacrylate. J Environ Chem Eng 2:293–303. https://doi.org/10.1016/j.jece.2013.12.015

Saha S, Basu H, Rout S, Pimple MV, Singhal RK (2020) Nano-hydroxyapatite coated activated carbon impregnated alginate: a new hybrid sorbent for uranium removal from potable water. J Environ Chem Eng 8:103999. https://doi.org/10.1016/j.jece.2020.103999

Singhal P, Vats BG, Pulhani V (2020) Magnetic nanoparticles for the recovery of uranium from seawater: challenges involved from research to development. J Ind Eng Chem 90:17–35. https://doi.org/10.1016/j.jiec.2020.07.035

Tag El-Din AF, Elshehy EA, Abd El-Magied MO, Atia AA, El-Khouly ME (2018a) Decontamination of radioactive cesium ions using ordered mesoporous monetite. RSC Adv 8:19041–19050. https://doi.org/10.1039/C8RA02707B

Tag El-Din AF, Elshehy EA, El-Khouly ME (2018b) Cellulose acetate/EDTA-chelator assisted synthesis of ordered mesoporous HAp microspheres for efficient removal of radioactive species from seawater. J Environ Chem Eng 6:5845–5854. https://doi.org/10.1016/j.jece.2018.09.005

Tang X, Zhou L, Le Z, Wang Y, Huang G, Adesina AA, Liu Z (2020) Preparation of porous chitosan/carboxylated carbon nanotube composite aerogels for the efficient removal of uranium(VI) from aqueous solution. Int J Biol Macromol 160:1000–1008. https://doi.org/10.1016/j.ijbiomac.2020.05.179

Tony MA, Lin LS (2021) iron coated-sand from acid mine drainage waste for being a catalytic oxidant towards municipal wastewater remediation. Int J Environ Res 15:191–201. https://doi.org/10.1007/s41742-020-00309-7

Torrik E, Soleimani SM, Ravanchi MT (2019) Application of kinetic models for heavy metal adsorption in the single and multicomponent adsorption system. Int J Environ Res 13:813–828. https://doi.org/10.1007/s41742-019-00219-3

Tufail M (2012) Radium equivalent activity in the light of UNSCEAR report. Environ Monit Assess 184:5663–5667. https://doi.org/10.1007/s10661-011-2370-6

Wu S, Wang L, Zhang P, El-Shall H, Moudgil B, Huang X, Zhao L, Zhang L, Feng Z (2018) Simultaneous recovery of rare earths and uranium from wet process phosphoric acid using solvent extraction with D_2EHPA. Hydrometallurgy 175:109–116. https://doi.org/10.1016/j.hydromet.2017.10.025

Yousef LA, Bakry AR, Abd El-Magied MO (2020) Uranium(VI) recovery from its leach liquor using zirconium molybdophosphate composite: kinetic, equilibrium and thermodynamic studies. J Radioanal Nucl Chem 323:549–556. https://doi.org/10.1007/s10967-019-06871-5